The liquid-glass transition: a mode-coupling perspective

1999 J. Phys.: Condens. Matter 11 A95

(http://iopscience.iop.org/0953-8984/11/10A/006)

J. Phys.: Condens. Matter **11** (1999) A95–A117. Printed in the UK PII: S0953-8984(99)00075-2

The liquid–glass transition: a mode-coupling perspective

H Z Cummins

Physics Department, City College of the City University of New York, New York, NY l0031, USA

Received 2 October 1998

Abstract. We review the dynamics of supercooled liquids approaching the liquid–glass transition, starting with the conventional generalized hydrodynamics formulation. Empirical models for the memory function are discussed, as are empirical models for the self-energy function for phonons in crystals. Two examples of microscopic analyses based on non-linear interactions are then described, the anharmonic lattice dynamics model for structural phase transitions, and Kawasaki's mode–mode-coupling approach for critical dynamics. We then review the mode-coupling theory of the liquid–glass transition, emphasizing its relation to generalized hydrodynamics with the memory function derived from a microscopic theory of non-linear interactions. We discuss the major predictions of this theory, particularly the asymptotic expansion results, which provide specific formulae for analysing experimental data.

1. Introduction

Although the liquid–glass transition resembles a second-order phase transition, with the liquid transforming continuously into an amorphous solid with no latent heat, it exhibits no diverging correlation length, symmetry change, or obvious order parameter. It is therefore generally not considered as a conventional thermodynamic phase transition and is better understood as a dynamical phenomenon, an ergodic–non-ergodic transformation related to a singularity in the underlying dynamics. The challenge has been to find a theoretical framework capable of predicting such a transformation and of simultaneously providing a detailed description of the relaxation dynamics of liquids and its evolution with decreasing temperature.

In 1984, Bengtzelius, Götze and Sjölander [1] and Leutheusser [2] showed that a particular version of a mode-coupling theory of liquids could lead to a dynamical singularity with characteristics resembling those of the liquid–glass transition. Subsequent analysis of this theory (now usually called MCT) by Götze and Sjögren and co-workers led to several detailed predictions for the dynamics of supercooled liquids which have stimulated much of the recent research in the glass transition field. One notable characteristic of the new approach is an extension of interest from the very slow structural relaxation close to the calorimetric glass transition temperature T_G, to include higher frequencies and higher temperatures, bringing into play a number of new experimental approaches. In his talk given as part of the Workshop to which this Special Issue is devoted, Wolfgang Götze reviewed some of the recent experiments that have provided crucial tests of MCT.

In this article I will present an introduction to MCT from an experimentalist's point of view, with no claim to completeness or mathematical rigour. The goal will be to consider MCT in the context of some earlier ideas, and then to describe how MCT leads to some of its specific predictions. Detailed discussions of the theory can be found by the interested reader in, e.g., references [3] and [4].

0953-8984/99/SA0095+23$19.50

1.1. The relaxation function

The shear viscosity η_s of liquids capable of being supercooled without crystallizing increases from $\sim 10^{-2}$ P at temperatures well above the melting temperature T_M, to 10^{13} P at the calorimetric glass transition temperature T_G. Maxwell's theory of viscoelasticity predicted that the characteristic α-relaxation time τ_α required for the local structure to relax to equilibrium after sudden application of a shear strain would increase with η_s as $\tau_\alpha = \eta_s / G_\infty$ where G_∞ is the high-frequency shear modulus. Many experimental studies with stress relaxation, dielectric susceptibility, ultrasonics, and other techniques have verified the predicted rapid increase of τ_α with decreasing T. However, in place of the single-exponential relaxation assumed by Maxwell, the α-process relaxation function $\phi(t)$ (also called a correlation function) is generally found to be better described by a stretched-exponential (Kohlrausch) function.

As experimental techniques evolved and measurements were extended to shorter times (or higher frequencies), it was found that there is also some fast relaxation preceding the onset of the final α-relaxation. These observations suggest that the relaxation function, normalized to $\phi(0) = 1$, might be represented approximately by

$$\phi(t) = (1 - f)g(t) + f \exp\left[-(t/\tau_\alpha)^\beta\right] \tag{1}$$

where f is the level at which the alpha relaxation begins. A schematic version of $\phi(t)$ is shown in figure 1 where, on a linear timescale, only the slow α-relaxation is visible, while on a logarithmic timescale the fast relaxation can also be seen.

With decreasing T, the slow relaxation moves to longer times, eventually 'freezing in' with the result that the plateau around region B in figure 1 effectively extends to infinity,

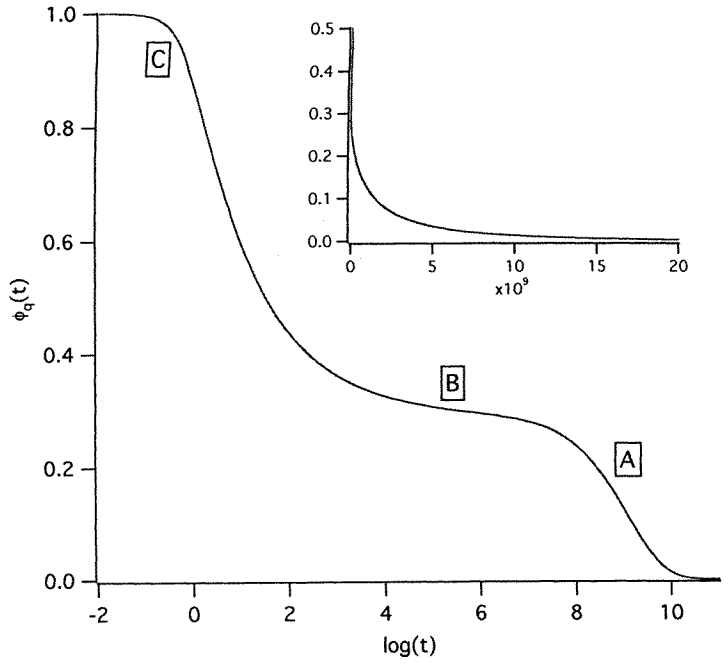

Figure 1. A schematic plot of $\phi_q(t)$ versus $\log(t)$ for a moderately supercooled liquid; (A) the long-time α-relaxation region; (C) the short-time (microscopic) region; (B) the intermediate region exhibiting two-step relaxation. Inset: on a linear timescale, only the final α-relaxation region is visible.

resulting in elastic scattering of neutrons or light. With further decrease of T (ignoring quantum fluctuations), the amplitude of the fast relaxation $(1 - f)$ decreases, so that of the frozen-in component has to increase: $f \to 1$ as $T \to 0$.

The relaxation function $\phi(t)$ represented in figure 1 or its Fourier transform $S(\omega)$ (whose real part is the power spectrum) has been investigated with many experimental techniques. Frequently, experimental data have been analysed with equation (1) with the fast-relaxation component $g(t)$ represented by some convenient phenomenological function such as exponential relaxation. In the simplest 'minimal model', $g(t)$ is attributed entirely to vibrational dynamics. It is extracted from low-temperature spectra where relaxation is presumably frozen out, and is assumed to be independent of temperature. While this minimal model of α-relaxation plus vibration does not generally provide accurate fits of experimental data [5], it is worth noting that such models do qualitatively predict two principal features of the dynamics as reflected in the susceptibility spectra $\chi''(\omega)$. If the fast relaxation $g(t)$ decays after a time t_f and is followed by the α-relaxation, there will generally be a susceptibility minimum. At low T, when the α-decay has moved to extremely long times with the result that the fast decay is followed by an extended plateau before the onset of the α-decay, the spectrum will be flat (white) for a range of frequencies below $\omega_f = 1/t_f$, and $\chi''(\omega)$ in this region will be proportional to ω. The resultant downward bending of the susceptibility spectrum at ω_f will produce a 'knee' at low temperatures. The susceptibility minimum and the knee are therefore very general predictions of any two-step decay model. The challenge to theory is that of correctly predicting their shape and temperature dependence.

1.2. Equations of motion: liquids

In simple liquids, classical hydrodynamics describes the density fluctuations $\delta\rho(r, t)$ by an equation of motion for the Fourier components $\rho_q(t)$ or for $\phi_q(t)$, the normalized autocorrelation function of $\rho_q(t)$:

$$\phi_q(t) = \langle \rho_q(t)\rho_q^*(0)\rangle / \langle |\rho_q|^2 \rangle \tag{2}$$

as

$$\ddot{\phi}_q(t) + \gamma_q \dot{\phi}_q(t) + \omega_q^2 \phi_q(t) = 0 \tag{3}$$

where $\omega_q = cq$, c is the adiabatic speed of sound, and $\gamma_q \propto q^2$ is the sound attenuation coefficient. Temperature (entropy) fluctuations, which couple to the density via thermal expansion, are ignored here for the sake of simplicity. From equation (3) the density-fluctuation spectrum $I_q(\omega)$ can be computed using either

$$I(\omega) = \frac{I_0}{\omega}\chi''(\omega) \tag{4}$$

which is the low-frequency version of the fluctuation-dissipation theorem, or else, equivalently, with the Wiener–Khintchine theorem

$$I(\omega) = \frac{I_0}{\pi}\mathrm{Re}[\phi(s)] \tag{5}$$

where $\phi(s)$ is the Laplace transform of $\phi(t)$. From equation (3) we find

$$I(\omega) = \frac{I_0\gamma_q}{(\omega_q^2 - \omega^2)^2 + (\omega\gamma_q)^2} \tag{6}$$

which, for $\gamma_q \ll \omega_q$, is the conventional Brillouin doublet consisting of peaks at $\pm\omega_q$ with half-width $\gamma_q/2$. For liquids possessing relaxation dynamics, equation (3) can be generalized by replacing the damping constant γ_q with a frequency-dependent damping

function $\Gamma_q(\omega) = \gamma_q + m_q(\omega)$. Mountain [6] first used this procedure with the relaxing degree of freedom responsible for $m_q(\omega)$ represented by the Maxwell–Debye single-exponential relaxation form

$$\Gamma_q(\omega) = \gamma_q + \mathrm{i}\tau\Delta_q^2/(1 - \mathrm{i}\omega\tau) \tag{7}$$

with which the spectrum

$$I(\omega) = I_0(\omega_q^2/\pi)\frac{\gamma_q + m_q''(\omega)}{[\omega^2 - \omega_q^2 + \omega m_q'(\omega)]^2 + [\omega\{\gamma_q + m_q''(\omega)\}]^2} \tag{8}$$

becomes

$$I(\omega) = \frac{I_0[\gamma_q + \Delta_q^2/(1 + \omega^2\tau^2)]^2}{[\omega_q^2 - \omega^2 + \omega^2\Delta_q^2\tau^2/(1 + \omega^2\tau^2)]^2 + [\omega\gamma_q + \omega\tau^2\Delta_q^2/(1 + \omega^2\tau^2)]^2}. \tag{9}$$

Equation (9) predicts that when $\omega_q\tau \gg 1$, the spectrum consists of a triplet: the two Brillouin components plus a new quasielastic feature, the 'Mountain peak', which is the α-peak of the density correlator in the hydrodynamic regime. Equation (3) can be further generalized by replacing the frequency-dependent part of $\Gamma(\omega)$ with a more elaborate function (such as the Kohlrausch or Cole–Davidson function) and replacing ω_q by a general frequency Ω_q. Then equation (3) becomes

$$\ddot{\phi}_q(t) + \Omega_q^2\phi_q(t) + \int_0^t \mathrm{d}t'\, M_q(t - t')\dot{\phi}_q(t') = 0. \tag{10}$$

Equation (10) has frequently been used as the starting point for the analysis of experimental data, with the memory function $M_q(t)$ modelled with various parametrized empirical functions. While such generalized hydrodynamics approaches can often provide excellent fits to experimental data, they produce no insight into the physical processes responsible for the form and the strong temperature dependence of the dynamics. What is missing in these approaches is a theory of $M_q(t)$.

1.3. Equations of motion: solids

In the conventional harmonic theory of lattice dynamics, the potential energy is initially truncated, retaining only terms quadratic in the atomic displacements. The resulting equations of motion can be diagonalized, yielding the lattice vibration modes, each with wavevector $\vec{q}$ and vibrational frequency $\Omega_{\vec{q}}$. (In the following, the quantities $\vec{q}$ will not be explicitly represented as vectors.) Each mode can be characterized by a Green's function or phonon propagator which, in this harmonic approximation, is

$$G_0(q, \omega) = \frac{2\omega/\beta\overline{h}}{\Omega_q^2 - \omega^2}. \tag{11}$$

This 'bare' harmonic Green's function can be modified to include anharmonic interactions by computing, via perturbation theory, the complex self-energy function $\Sigma(q, \omega)$ with which the phonon propagator becomes

$$G(q, \omega) = \frac{2\omega/\beta\overline{h}}{\Omega_q^2 - \omega^2 + 2\Omega_q\Sigma(q, \omega)}. \tag{12}$$

The self-energy $\Sigma(q, \omega)$ produces damping through its imaginary part and a frequency shift through its real part.

Axe *et al* [7] introduced a phenomenological self-energy function

$$\Sigma(q, \omega) = -\mathrm{i}\omega\delta^2/(\gamma - \mathrm{i}\omega)$$

to explain the central-peak phenomenon, a narrow quasielastic feature appearing in the neutron and light scattering spectra of crystals undergoing structural phase transitions. This is an exact analogue of Mountain's approach for liquids described above. Winterling [8] first used this relaxing self-energy approach for glasses in order to explain the excess low-frequency light scattering intensity observed in the Raman spectrum of vitreous silica. He used the same empirical memory function as was used by Axe *et al*, combined with a sum over modes often employed for amorphous solids because their normal modes are not spatially periodic. Winterling wrote

$$\frac{I(\omega)}{\omega[n(\omega,T)+1]} \propto \sum_q C_b(q)\frac{1}{\omega}\mathrm{Im}[D(q,\omega)] \tag{13}$$

where $C_b(q)$ is an optical coupling constant, and

$$D(q,\omega) = \{\omega^2 - \omega_0^2(q)[1 - \mathrm{i}g\omega\tau/(1-\mathrm{i}\omega\tau)]\}^{-1}. \tag{14}$$

Winterling's approach has been elaborated in a series of papers by Sokolov and co-workers [9] with the relaxing part of $D(q,\omega)$ taken as the Debye function (as in equation (14)) with the amplitude and relaxation time treated as free fitting parameters. Here, as for supercooled liquids, good fits to experimental data can be obtained, and the approach is a promising way to view the liquid–glass transition from the glass side.

2. Non-linear effects

Equations (10) and (12) can be shown to be formally exact, with all the unknown physics hidden in the memory kernel $M_q(t)$ or the phonon self-energy $\Sigma(q,\omega)$. While data fitting can be carried out using empirical fitting functions, the real challenge is to find a method for deriving these functions rather than simply guessing at their form. In this section we recall briefly two examples from the field of critical phenomena that suggest a more fundamental way to proceed, based on treatments of non-linear interactions.

2.1. Structural phase transitions

The first example is that of second-order structural phase transitions in which a crystal spontaneously destabilizes on cooling through a critical temperature T_C and transforms continuously to a new lower-symmetry structure. Such transitions are characterized by a 'soft mode', a lattice vibration whose frequency decreases with decreasing temperature, reaching $\Omega = 0$ at $T = T_C$. Since a necessary condition for the stability of crystals is that $\Omega_q^2 > 0$ for all vibrational modes, the soft mode can be considered as the origin of the instability that drives the displacive phase transition.

The phonon self-energy function $\Sigma(q,\omega)$ of equation (12) can be calculated approximately via anharmonic lattice dynamics [10]. As shown schematically in figure 2(a), cubic anharmonicity causes the phonon q to decay into two new phonons, q_1 and q_2, which produces damping or a finite phonon lifetime. The same interaction in second order, as shown in figure 2(b), is the leading contribution to the self-energy. The summation of such diagrams leads to an expression for $\Sigma(q,\omega)$ from which the temperature-dependent phonon properties can be found. Such calculations require as input only the equilibrium structure and the interatomic potentials.

The application of this anharmonic phonon theory technique to displacive phase transitions begins with the observation that for the crystal structure that is stable at high temperature, the harmonic solutions may show that, for some mode, $\Omega_q^2 < 0$; the high-temperature structure would therefore be unstable at $T = 0$. However, since the anharmonic contributions cause

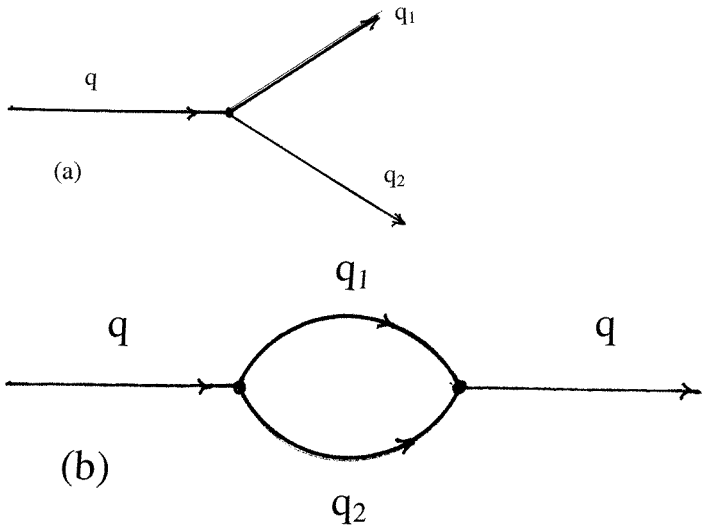

Figure 2. Anharmonic phonon interaction effects. (a) Lowest-order cubic anharmonic decay of a phonon q into two phonons q_1 and q_2. (b) The leading contribution to the self-energy $\Sigma(q,\omega)$ of the phonon q with intermediate two-phonon states q_1, q_2.

$\Sigma(q,\omega)$ to increase with increasing T, the renormalized resonance frequency (i.e. the ω for which the denominator in equation (12) vanishes) may be positive at high temperatures. Thus T_C corresponds to the temperature at which $\Omega_q^2 + 2\,\mathrm{Re}[\Omega_q \Sigma(q,\omega)]$ decreases to 0 with decreasing T, from which the soft-mode behaviour follows.

Calculation of the full self-energy function is impossible since it requires summing over infinitely many diagrams. However, the leading-order self-energy diagram of figure 2(b) can already approximate the full solution if the initial mode q and the two intermediate-state modes q_1 and q_2 are treated self-consistently [11]. So the dynamical process underlying structural phase transitions can be understood as anharmonic phonon interactions which renormalize not only the 'primary' phonon q, but all phonons self-consistently. This, in very simplified form, is the anharmonic lattice dynamics explanation of structural phase transitions. While this formulation does not provide accurate quantitative predictions for the temperature dependence of the soft-mode frequency, it does capture the origin of the instability and resulting phase transition. Note that in this approach there is no 'built-in' anomaly. Without the anharmonic terms the vibrational modes would remain purely harmonic with their $T = 0$ frequencies, and exhibit no temperature dependence.

2.2. The liquid–vapour critical point

The second example that we consider is Kawasaki's mode–mode-coupling theory for the liquid–vapour critical point. Liquids, lacking atomic equilibrium positions and the regular spatial structure of crystals, cannot be described by the theory of lattice vibrations (although a related approach called instantaneous normal-mode analysis has been pursued by some authors). Liquid dynamics is usually formulated in terms of kinetic equations which include some basic assumptions such as the separation of fast and slow variables. A general theory of liquid dynamics, due to Mori and Zwanzig, expresses the equation of motion of a dynamical

variable $A(t)$ as a generalized Langevin equation:

$$\frac{\mathrm{d}A}{\mathrm{d}t} = \mathrm{i}\Omega A(t) - \int_0^t \mathrm{d}\tau\ K(\tau)A(t-\tau) + F(t). \tag{15}$$

The quantity Ω and the functions $K(t)$ and $F(t)$ are designated as the frequency, memory function, and random force, respectively, and are formally determined exactly by the Liouville operator. (For a description of the Zwanzig–Mori formalism, see e.g., [12].) The memory function $K(t)$ is proportional to $\langle F(t)F^*(0)\rangle$, the correlation function of the random force. Equation (15) can be extended to a set of variables $(A_1, A_2, \ldots, A_n)$; A and $F(t)$ then become column vectors while Ω and $K(t)$ become matrices. Equation (15) simplifies if all the slow variables are included in $A(t)$, while the random forces $F(t)$, which include all of the fast variables, have correlation functions which decay very rapidly such that $K(t) = 2\pi\gamma\delta(t)$.

Kawasaki introduced a crucial extension of the Zwanzig–Mori formalism for systems near a critical point [13]. Close to a critical point, fluctuations become very large, and non-linear interactions can become important. Fixman [14] had first considered how such non-linear interactions would modify sound waves, entropy fluctuations, concentration fluctuations, and transverse velocity modes near T_C. Kawasaki constructed a formal theory of these non-linear effects by extending the set of slow variables A to include products A_iA_j as additional slow variables. He then separated the ordinary single variables $A_j(t)$ and the product variables $A_{q'}(t) = A_{q1}A_{q2}$ to obtain

$$\frac{\mathrm{d}A_q(t)}{\mathrm{d}t} = (\mathrm{i}\Omega_q - \Gamma_q)A_q(t) + (\mathrm{i}\Omega_{q'} - \Gamma_{q'})A_{q'}(t). \tag{16}$$

In order to calculate correlation functions of the $A_q(t)$

$$\phi_q(t) = \langle A_q(t)A_q^*(0)\rangle \tag{17}$$

the product variables must be eliminated. This was done formally via the Mori–Zwanzig approach which produces four-point correlation functions. Kawasaki factorized these four-point functions into products of two-point correlation functions (the factorization approximation) and found the following equation of motion for $\phi_q(t)$:

$$\frac{\mathrm{d}\phi_q(t)}{\mathrm{d}t} = \mathrm{i}\Omega_q\phi_q(t) + \int_0^t \mathrm{d}t'\ K_q(t')\phi_q(t-t') \tag{18}$$

where the memory function $K_q(t)$ is given by

$$K_q(t) = \sum_{q_1,q_2} V(q, q_1, q_2)\phi_{q_1}(t)\phi_{q_2}(t). \tag{19}$$

The power of this approach is that the coupling constants V in equation (19) can be calculated with the projection operator formalism. Thus, a set of closed equations are found, permitting quantitative evaluation of the effects due to the non-linear interactions.

From these equations, Kawasaki evaluated the contributions of diagrams beginning with ones like that of figure 2(b). The results provided quantitative predictions for various dynamical properties near the critical point that were extensively tested and often found to provide excellent agreement with experimental measurements. A striking result of Kawasaki's analysis was the prediction of critical anomalies in transport coefficients, a result not anticipated in earlier theories of critical phenomena. These anomalies occur when a transport mode, e.g. a thermal diffusion mode, is considered as the primary mode q in the non-linear dynamical equations, and one of the two modes in the intermediate two-mode state is the order-parameter mode, e.g. a density-fluctuation mode for the liquid–vapour critical point.

Note that these transport anomalies are secondary consequences of the growing fluctuations in the order parameter as T approaches T_C. For the liquid–vapour critical point,

for example, the amplitude of the density fluctuations $\rho_q(t)$ diverges as $T \to T_C$. The new transport anomalies predicted by Kawasaki's mode–mode-coupling approach are due to the non-linear effects of these growing fluctuations and of the static susceptibilities, which are built into the calculations from the outset.

3. Mode-coupling theory of the liquid–glass transition

3.1. The MCT equations and their solutions

MCT begins with the equation of motion (10) for the normalized density correlation function $\phi_q(t)$ which can be derived from the Zwanzig–Mori formalism [3]:

$$\ddot{\phi}_q(t) + \Omega_q^2 \phi_q(t) + \int_0^t \mathrm{d}t'\, M_q(t-t')\dot{\phi}_q(t') = 0 \tag{20}$$

where the memory kernel $M_q(t)$, the correlation function of the fluctuating force $F_q(t)$, is then separated into a 'fast' (regular) component $\gamma_q \delta(t)$ and a time-dependent part $\Omega_q^2 m_q(t)$. (The frequency $\Omega_q^2 = q^2 v^2 / S_q$ is the normalized second moment of $S(q,\omega)$, v is the thermal velocity, and S_q denotes the static structure factor.) Equation (20) then becomes

$$\ddot{\phi}_q(t) + \gamma_q \dot{\phi}_q(t) + \Omega_q^2 \phi_q(t) + \Omega_q^2 \int_0^t m_q(t-t')\dot{\phi}_q(t')\,\mathrm{d}t' = 0. \tag{21}$$

Since the fluctuating force occurs primarily between pairs of particles, the dominant contribution to $F_q(t)$, the Fourier transform of $F(r_{12})\,\delta\rho(r_1,t)\,\delta\rho(r_2,t)$, can be approximated as a sum of density-fluctuation pairs $\rho_{q1}(t)\rho_{q2}(t)$ with $q_1 + q_2 = q$. With Kawasaki's factorization approximation applied to the resulting four-point correlators, one obtains for the leading-order contribution to $m_q(t)$

$$m_q(t) = \frac{1}{2} \int\int \frac{\mathrm{d}^3 q_1\, \mathrm{d}^3 q_2}{(2\pi)^6}\, V(q,q_1,q_2)\phi_{q_1}(t)\phi_{q_2}(t)\delta(q+q_1+q_2). \tag{22}$$

The vertices (or coupling constants) $V(q,q_1,q_2)$ are completely determined by the static structure factors S_q via

$$V(q,q_1,q_2) = (n/q^4) S_q S_{q_1} S_{q_2} [\vec{q}\cdot\vec{q}_1 C_{q_1} + \vec{q}\cdot\vec{q}_2 C_{q_2}]^2. \tag{23}$$

(C_q is the direct correlation function, related to S_q by $S_q = 1/[1 - nC_q]$, and n is the density.)

Note that equation (23) for the coupling constants V contains only the static structure factors and not the intermolecular potentials. This is a crucial simplification since for some potentials (e.g. hard spheres) the potential is singular, but the structure factors are nevertheless well behaved. The origin of this simplification lies in treating the fluctuating force not as the gradient of the intermolecular potential (which may be undefined), but instead, via Newton's equation, as the time derivative of the current. One then finds, with the use of Yvon's theorem, that projecting the random force onto pairs of density-fluctuation modes yields equations (22) and (23) [3].

Equations (21), (22), and (23) constitute the basic (or idealized) version of MCT, given as a closed set of equations. If the intermolecular potential is known, the structure factors can be computed with well-established approximation methods (e.g. the Percus–Yevick equation) and used to evaluate the vertices $V(q,q_1,q_2)$. The equations are then solved self-consistently for a discrete set of wavevectors (typically 100 to 400).

Before discussing MCT further, we want to emphasize two essential aspects of these equations. First, equation (20) is identical to the generalized hydrodynamics equation (8). However, rather than substituting an empirical function with adjustable parameters for $m_q(t)$,

a formal procedure is given by equations (22) and (23) for its computation with no free parameters. The origin of the resulting 'generalized damping function' is a direct analogue of the non-linear phonon decay process of figure 2(a) since the density-fluctuation mode ϕ_q decays into the two-mode state $\phi_{q1}\phi_{q2}$ via the non-linear interaction represented by the vertex $V(q, q_1, q_2)$ of equation (23).

Second, the MCT equation (20) and the method of evaluating the vertices is formally equivalent to Kawasaki's mode–mode-coupling theory discussed briefly in section 2. However, there is a profound difference between the implementation and results of the two theories. In Kawasaki's analysis, the anomalous behaviour of mode q_1 arises because one of the two other modes with which it couples is already anomalous, and because the vertices themselves diverge with the static susceptibility. In MCT, however, before the non-linear interactions are included, all of the modes are regular, and finite-order perturbation theory does not produce a singularity. The interesting new physics emerges only when the equations are solved self-consistently so that modes q, q_1, and q_2 are all treated on an equal footing. As T is varied, the structure factors vary smoothly with q and T. The singularity in the solutions of equation (21) appears spontaneously at some critical value T_C as a zero-frequency pole in the Fourier transform of $\phi_q(t)$ for all q simultaneously. This is the central, unexpected discovery at the heart of MCT.

A numerical solution of the full MCT equations was first carried out for a system of particles interacting via a Lennard-Jones potential by Bengtzelius [15] and has also been performed for the hard-sphere system [16, 17]. Most recently, it has been used for the Baxter model of sticky hard spheres by Fabbian *et al* [18].

Numerical solutions of the MCT equations for the hard-sphere system with structure factors calculated via the Percus–Yevick equation are shown for two q-values in figure 3 (from Franosch *et al* [16]). The different curves represent different packing fractions ϕ labelled with the index n, where $\phi = \phi_c(1+e)$ and $e = \pm 10^{-n/3}$. The result for the critical packing fraction ϕ_c is indicated by the dark curve labelled c. Note that for $\phi \geqslant \phi_c$, the correlators do not decay to zero.

A remarkable aspect of MCT is that, in the weak-coupling limit (high T or low density), solutions of the MCT equations (21) yield only the damped harmonic oscillator results. As ϕ increases, the non-linear coupling causes the correlation functions $\phi(t)$ to stretch out to longer times, generating not only some non-trivial intermediate-time dynamics, but the final α-relaxation as well. Thus, the full $\chi''(\omega)$ (shown in figure 7—see later), apart from the high-frequency microscopic peak, is entirely due to the non-linear interactions. This result is fundamentally different from the many empirical models in the literature in which the α-peak, some 'fast process', and a microscopic peak are added together, each containing some free parameters which can then be adjusted arbitrarily to fit experimental data.

Ideally, the ability of MCT to correctly describe the dynamics of supercooled liquids approaching the glass transition could be tested directly by comparing the numerically obtained correlation functions, or the corresponding power spectra $S(q, \omega)$ or susceptibility spectra $\chi_q''(\omega)$ directly to experimental data. This procedure has been partially carried out, for colloids and computer simulations, to be discussed in this Special Issue by Gotze. However, liquids composed of atoms or simple molecules generally crystallize rather than forming glasses, while real glass-forming materials have intermolecular potentials which are too complicated to allow accurate evaluation of the coupling coefficients. Therefore, most experimental tests of MCT have been carried out either by comparison with simple schematic versions of MCT, or with particular general predictions of the theory obtained from asymptotic expansions. We consider these general MCT predictions in the following sections. A brief description of the asymptotic analysis is given in the appendix.

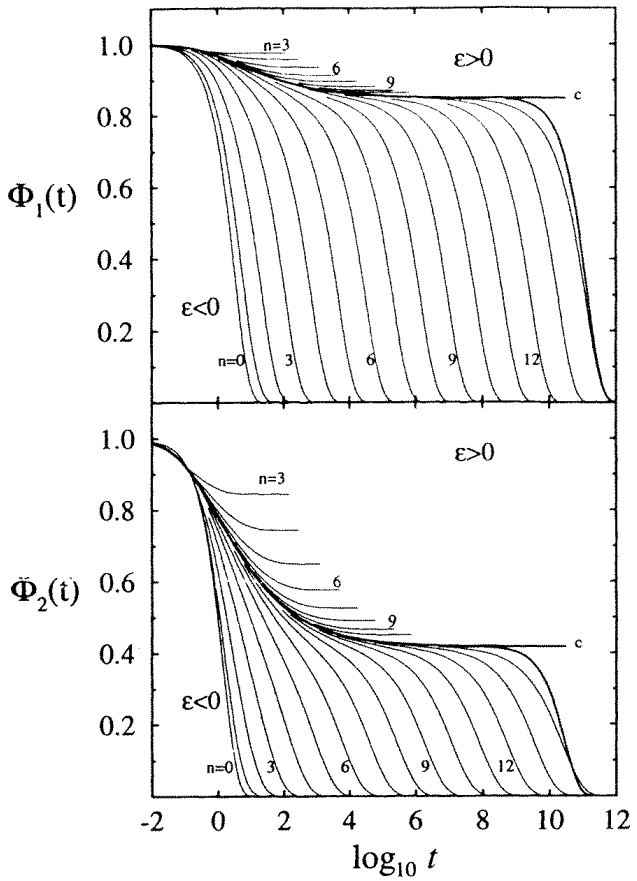

Figure 3. Solutions to the MCT equations for a hard-sphere system at two wavevectors $q_1 = 7.0$ and $q_2 = 10.6$. The unit of length is chosen such that the particle diameter is unity. The dark curves labelled c are at the critical packing fraction ϕ_c. The other curves are labelled with an index n where $\phi = \phi_c(1 + \epsilon)$ and $\epsilon = \pm 10^{-n/3}$. Exponential fits to the $n = 14$ curves are shown by the dark curves on the right. (From reference [16].)

3.2. Glass transition singularities

The $t \to \infty$ limit of $\phi_q(t)$ is called the non-ergodicity parameter $f_q(T)$. At high temperatures, where the coupling constants $V(q, q_1, q_2)$ in equation (22) are small, $\phi_q(t)$ decays to zero rapidly following the initial microscopic transient. The system is ergodic, and $f_q = 0$. With decreasing T, the coupling constants increase smoothly, until the glass transition singularity is reached where $\phi_q(t)$ no longer decays to zero, even for infinite time. The density fluctuations are then partially frozen in, since $\phi_q(t)$ only decays from 1 to f_q with $0 < f_q \leqslant 1$. The system is then non-ergodic with the frozen-in density fluctuations producing elastic scattering. The non-ergodicity parameter f_q is equivalent to the Debye–Waller factor in crystals.

Smooth variation of the coupling constants with decreasing T (or increasing packing fraction) leads to a critical temperature T_C at which f_q changes discontinuously from zero to a non-zero critical value f_q^c. Solving the MCT equations for $t \to \infty$ and $T \to T_C$, one finds that, for $T < T_C$,

$$f_q(T) = f_q^c + h'_q\sqrt{\sigma} \tag{24}$$

where $\sigma \propto (T_C - T)/T_C$ is called the separation parameter. This square-root cusp in $f_q(T)$ is the first general prediction of MCT. Since, at $T = T_C$, $\phi_q(t \to \infty)$ jumps discontinuously from 0 to f_q^c, the dynamical singularity at T_C constitutes a bifurcation. Because there are many control parameters in the theory (all of the V_q), many types of bifurcation are technically possible. The type thought to be most relevant to the liquid–glass transition, the fold bifurcation, is what occurs in the solution of a polynomial equation when two solutions coalesce. The results discussed in this paper are appropriate for this case.

3.3. The two-step relaxation scenario

At high temperatures, solutions to the MCT equations have the form illustrated in figure 3 for $n = 0$ or 1. The short-time microscopic transient decays to zero (with or without damped oscillation) within a time window of about one decade. As T decreases, the microscopic transient is followed by decay towards a 'plateau', which is followed by a second decay ending in the familiar α-relaxation process. As T decreases further, the plateau extends to longer times as illustrated in figure 3 for, e.g., $n = 12$. This splitting off of the structural relaxation from the initial microscopic transient produces the two-step relaxation scenario in the region between the microscopic dynamics and the α-decay which has been observed in many experiments and computer simulations. In MCT, this region is designated the β-relaxation region.

The development of the intermediate two-step decay as T decreases reflects the growing strength of the 'cage effect', i.e. temporary localization of a particle in the transient cage formed by its neighbours. One can roughly view the sequence of dynamical regimes of the relaxation process as an initial microscopic motion of each particle within its transient cage followed, in the plateau region, by collective motion of the cage. The beginning of the decay away from the plateau, called the von Schweidler decay, corresponds to the initial break-up of the cages which is followed, finally, by the long-time α-relaxation.

The plateau level for $T > T_C$ is f_q^c, the value of $\phi_q(\infty)$ at $T = T_C$. As T approaches T_C, $\phi_q(t)$ remains close to f_q^c for increasingly longer times. Close to the bifurcation, where $(T - T_C)/T_C \ll 1$, the MCT equations can be expanded in the small parameter $\phi_q(t) - f_q^c$. Several central MCT predictions can then be derived analytically from this asymptotic analysis.

First, one finds that

$$\phi_q(t) - f_q^c = h_q G(t). \tag{25}$$

This factorization result predicts that the q-dependence of $\phi_q(t) - f_q^c$ in this asymptotic region is completely specified by h_q (which is trivially related to h'_q in equation (24)), while the time dependence of all correlators is given by the same q-independent function $G(t)$, which is called the β-correlator. $G(t)$ is the solution to the equation

$$\lambda G^2(t) + \sigma = \frac{\mathrm{d}}{\mathrm{d}t} \int_0^t G(t - t')G(t')\,\mathrm{d}t'. \tag{26}$$

Solving equation (26) for $\sigma < 0$ (liquid), one finds that $G(t)$ first decays to zero as t^{-a} (the critical decay), and then decreases as $-t^b$ (von Schweidler decay). The two exponents a and b are related to each other via an exponent parameter λ ($1/2 < \lambda < 1$) by

$$\lambda = \Gamma^2(1/a)/\,\Gamma(1 - 2a) = \Gamma^2(1 + b)/\,\Gamma(1 + 2b)$$

where $\Gamma(x)$ is the gamma function. Equation (25) is the leading-order asymptotic result usually employed in comparing experimental data with MCT. The exponent parameter λ is the only material-dependent quantity, and is usually treated as an adjustable fitting parameter. For the hard-sphere system, λ was calculated with the Percus–Yevick approximation to be $\lambda = 0.74$.

The solutions of equation (26) have different forms for $\sigma < 0$ (liquid) and $\sigma > 0$ (glass), as discussed below in section 3.4. For $\sigma = 0$ (i.e. $T = T_C$), equation (26) is solved by

$$G(t)_{\sigma=0} = (t_0/t)^a \tag{27}$$

where t_0 is a microscopic timescale of the order of 10^{-12} s for molecular liquids, determined by matching equation (25) to the microscopic transient. Thus, at $T = T_C$, the t^{-a} critical decay extends to $t = \infty$.

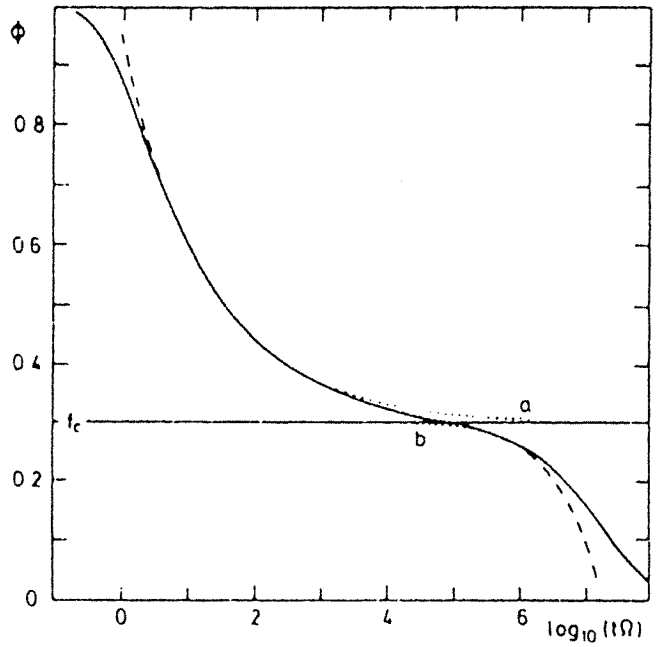

Figure 4. Comparison of the MCT solution for $\phi_q(t)$ (solid curve) with the asymptotic β-relaxation approximation (dashed curve) (equations (25) and (26)).The dotted curves show the two power laws. (From reference [4].)

Note that $\phi_q(t)$ given by equations (25) and (26) matches the full solution of the MCT equations only in the asymptotic region close to $\phi_q(t) = f_q^c$ as shown in figure 4. This asymptotic beta-correlator solution lacks both the short-time microscopic structure and the long-time α-relaxation structure which are, however, present in the full MCT solutions. Furthermore, the domain of validity of these leading-order asymptotic solutions cannot be established *a priori*. Recently, this domain-of-validity question has been addressed by Franosch *et al* [16] and Fuchs *et al* [19] who compared numerical solutions for the hard-sphere system with MCT fits using both leading-order and leading-order plus next-to-leading-order MCT solutions.

3.4. The two scaling regimes

Solutions to the MCT equations, such as those for hard spheres shown in figure 3, can be replotted in scaled form as shown in figure 5. In (a), the full solutions are shown; in (b), the scaling brings the β-relaxation regions into coincidence; in (c), the scaling brings the α-relaxation regions, including the von Schweidler decay, into coincidence. These plots illustrate the scaling regions of the MCT equations that can be found analytically from the asymptotic

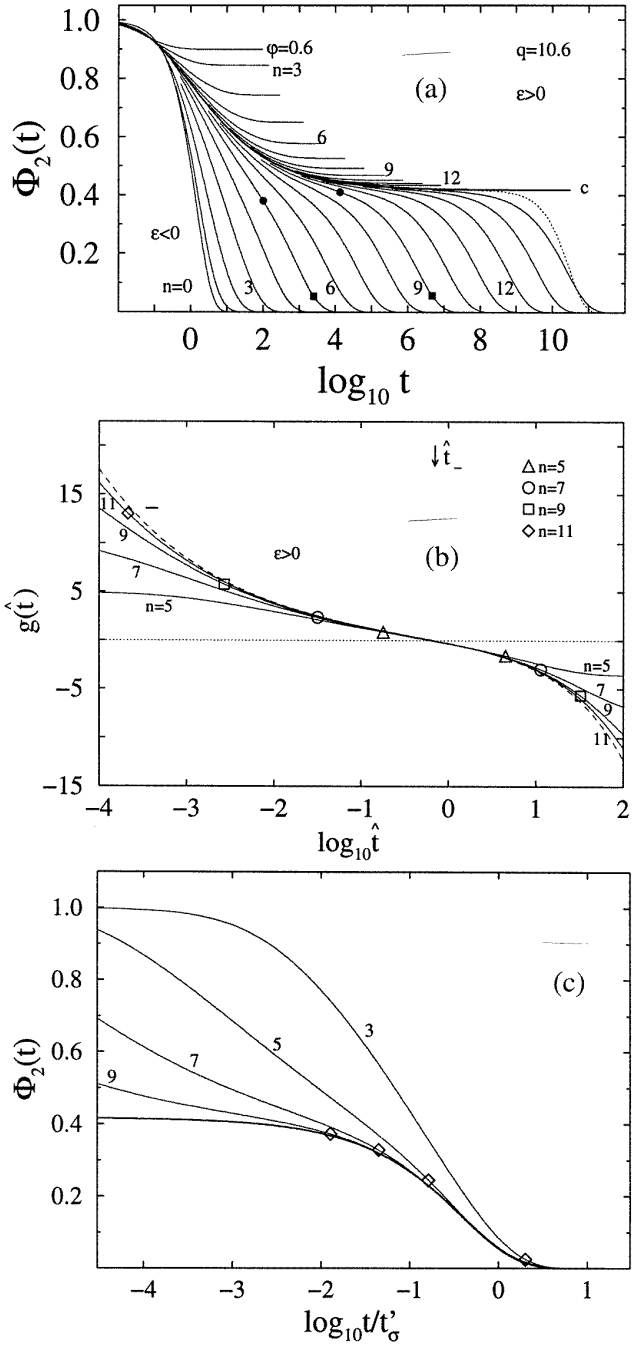

Figure 5. MCT solutions for the hard-sphere system for $q = 10.6$; (a) for unscaled time, as in figure 3; (b) with time scaled to t/t_σ; (c) with time scaled to t/t'_σ. The index n defines the packing fraction by $(\phi - \phi_c)/\phi_c = \pm 10^{-n/3}$. The solid circles and squares in (a) indicate the times t_σ and t'_σ respectively for $n = 5$ and 9. The dashed curve in (b) is the master function $g_-(\hat{t})$. The full curves show the rescaled correlators $\hat{\Phi}(\hat{t}) = (\phi_q(t/t_\sigma) - f_q^c)/h_q\sqrt{|\sigma|}$. The open symbols mark the positions where the correlators deviate from the master function by 20%. The heavy curve in (c) is the master function F^α and the open symbols mark the positions where ϕ_q and F differ by 20%. (Courtesy of M Mayr.)

solutions. They also illustrate that the scaling region increases rapidly with increasing n, i.e. as the packing fraction ϕ approaches ϕ_c, or T approaches T_C. Let us consider the two scaling laws in detail.

3.4.1. The first (β-) scaling regime. The β-correlator $G(t)$, defined by equation (26) for any selected value of λ, can be shown analytically to obey the scaling laws

$$G(t)_{\sigma<0} = \sqrt{|\sigma|}\, g_-(t/t_\sigma) \tag{28a}$$

$$G(t)_{\sigma>0} = \sqrt{|\sigma|}\, g_+(t/t_\sigma) \tag{28b}$$

where the scaling time t_σ is given by

$$t_\sigma = t_0/|\sigma|^{1/2a}. \tag{29}$$

The master functions $g_\pm(t/t_\sigma)$ are solutions to equation (26) with $\sigma = \pm 1$. Master functions $g_\pm(\hat{t}\,)$ for $\lambda = 0.735$, where the scaled time $\hat{t} = t/t_\sigma$, are illustrated in figure 6(a). For short times ($t \ll t_\sigma$), both master functions follow the critical decay law $g_\pm = \hat{t}^{-a}$. For longer times ($t \gg t_\sigma$), the liquid master function $g_-(\hat{t}\,)$ follows the von Schweidler law $g_-(\hat{t}\,) = -B\hat{t}^b$ while the glass master function $g_+(\hat{t}\,)$ has the constant value $1/\sqrt{1-\lambda}$. (When leading-order

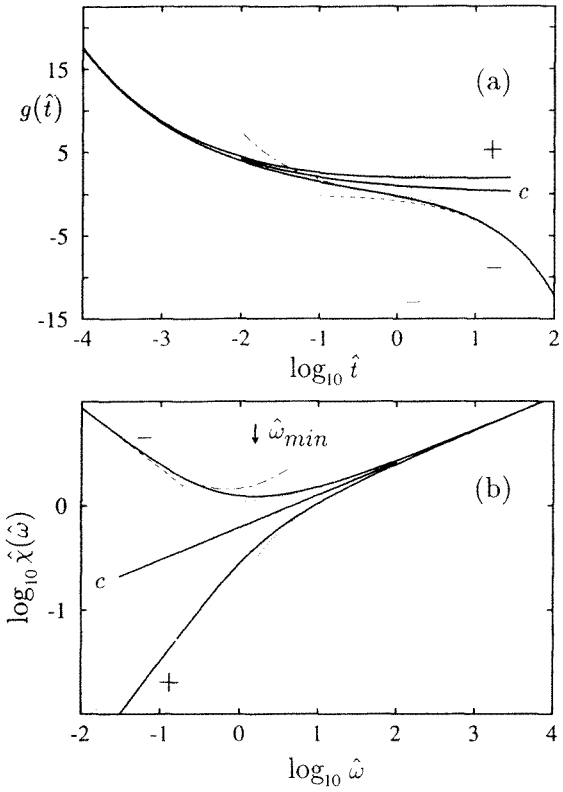

Figure 6. (a) Master functions $g_+(\hat{t})$ and $g_-(\hat{t})$ for $\lambda = 0.735$. The dashed curve shows the von Schweidler decay. The solid curve marked c is the critical correlator $\hat{t}^{-a}$. (b) Susceptibility master functions $\hat{\chi}(\hat{\omega})$ for $\lambda = 0.735$ illustrating the minimum and the knee. The solid curve marked c corresponds to the critical point where $\chi''(\omega) \propto \omega^a$. (From reference [16].)

corrections to the asymptotic scaling laws are included, these two power-law regimes are described by $\hat{t}^{-a}(1 + p\hat{t}^{-a})$ and $-B\hat{t}^{b}(1 + \sqrt{|\sigma|}p'\hat{t}^{b})$ [16].)

From the correlation functions $\phi_q(t)$, the power spectrum $S(q, \omega)$ is found by Fourier transformation, and the susceptibility spectrum $\chi''(\omega)$ follows by multiplying $S(q, \omega)$ by ω. The scaling laws for $\phi_q(t)$ also imply scaling laws for the susceptibility spectra as indicated in figure 7. The $\chi''(\omega)$ spectra in the β-relaxation region should scale as

$$\chi''_{\pm}(\omega) = h_q\sqrt{|\sigma|}\,\hat{\chi}_{\pm}(\omega t_\sigma). \tag{30}$$

The susceptibility master functions $\hat{\chi}_{\pm}$ for $\lambda = 0.735$ are shown in figure 6(b). For $T > T_C$, the form of the MCT $\chi''_{-}(\omega)$ function in the vicinity of the minimum is given approximately by the interpolation equation:

$$\chi''_{-}(\omega) = \chi''_{\min}\left[b\left(\frac{\omega}{\omega_{\min}}\right)^{a} + a\left(\frac{\omega_{\min}}{\omega}\right)^{b}\right]\frac{1}{a+b} \tag{31}$$

($\omega_{\min}$ is proportional to $\omega_\sigma = 1/t_\sigma$).

For both $T < T_C$ and $T > T_C$, $\chi''(\omega)$ should exhibit a critical-decay region of ω^a power-law behaviour for frequencies above the minimum but below the region of microscopic dynamics:

$$\chi''_{\pm}(\omega) \propto \omega^{a} \qquad (\omega_\sigma \ll \omega \ll \Omega_q). \tag{32}$$

(Note that if the region of microscopic dynamics is not sufficiently far away from $\omega_{\min}$, this critical decay region may be difficult to observe, and fits of experimental data to equation (32) can produce some a_{eff} which is unrelated to the critical exponent a.) For $\omega < \omega_\sigma$, the two $\hat{\chi}''(\omega)$ master curves are different. For $T > T_C$, the von Schweidler power-law behaviour is predicted:

$$\chi''_{-}(\omega) \propto \omega^{-b} \qquad (\omega_\alpha \ll \omega \ll \omega_\sigma) \tag{33}$$

where $\omega_\alpha = 1/\tau$ (τ is the second scaling time discussed in the following section). For $T < T_C$, a linear regime is predicted:

$$\chi''_{+}(\omega) \propto \omega \qquad (0 < \omega \ll \omega_\sigma). \tag{34}$$

For $T > T_C$, the two power-law regions ω^{-b} and ω^{a} are separated by the susceptibility minimum at $\omega_{\min}$. For $T < T_C$, the two power-law regions ω^{1} and ω^{a} should produce a slope change appearing as a downward-concave feature—the 'knee' (see figure 6(b)). We note that the existence of a 'knee' is not a unique feature of MCT. Any model for $\phi(t)$ at low temperatures (such as equation (1)) which includes fast-relaxation dynamics followed at a much longer time by the final α-relaxation can produce such a feature. The non-trivial MCT predictions concern the form and scaling properties of both the knee and the minimum. The knee, however, is strongly affected by activated hopping processes not included in this idealized version of MCT. We will discuss these effects further in the next section.

As T approaches T_C, the range of frequencies for which $\chi''(\omega)$ follows the scaling law (equation (30)) increases, as can be seen in figure 7(b). Therefore, in using MCT to analyse experimental data, the fitting range must be chosen so as not to exceed the scaling range. This point was discussed in detail by W Götze in his talk mentioned earlier.

3.4.2. The second (α-) scaling regime. As seen in figures 5(c) and 7(c), solutions to the MCT equations can also be scaled so that the α-decay regions of $\phi_q(t)$ or $\chi''_{-}(\omega)$ for different temperatures overlap. This α-scaling is the MCT equivalent of the conventional time–temperature superposition principle which asserts that relaxation spectra at different temperatures can be superimposed by scaling the time as t/τ where τ is the α-relaxation time.

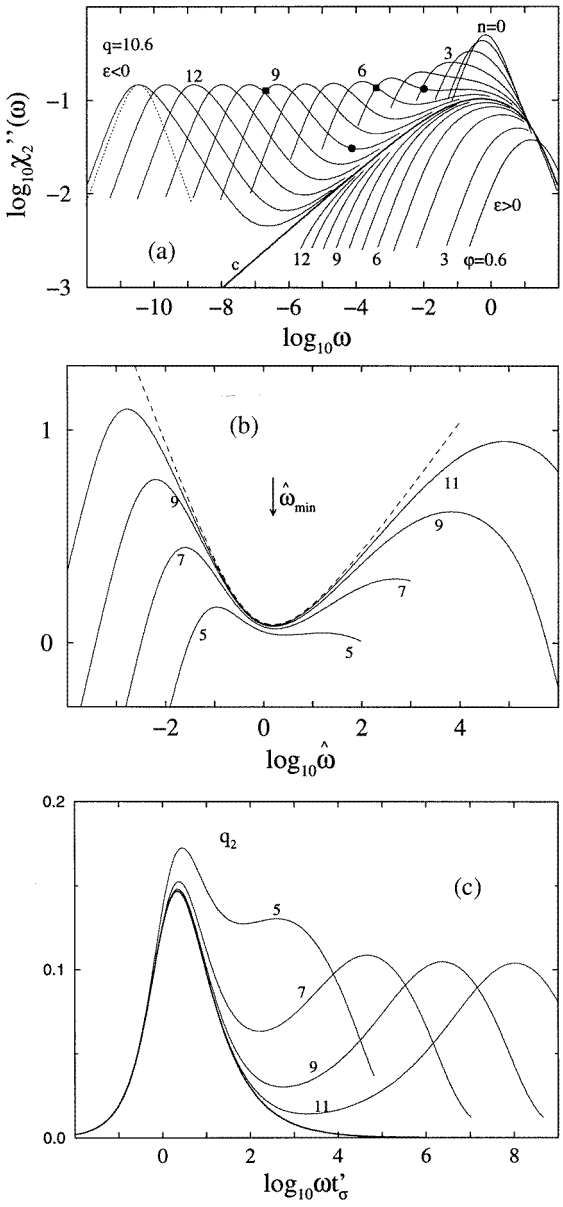

Figure 7. $\chi''(\omega)$ spectra for the hard-sphere system at $q = 10.6$ as in figure 5; (a) the unscaled frequency; (b) ω scaled to ω/ω_σ; (c) ω scaled to $\omega/\omega_{\sigma'} = \omega t'_\sigma$. (Courtesy of M Mayr.)

The long-time asymptotic analysis of the MCT equations for $\sigma < 0$ and $(T - T_C)/T_C \ll 1$ leads to the scaling relation

$$\phi_q(t) = F_q^\alpha(t/\tau) \qquad (t \gg t_\sigma). \tag{35}$$

The master function F_q^α is independent of T. It is determined by the vertices in equation (23) evaluated for $T = T_C$. In contrast to that in the β-relaxation region, $\phi_q(t)$ in this α-relaxation region has no universal form. Numerical solutions of the MCT equations show that the α-

relaxation can be described, to a good approximation, by the Kohlrausch stretched-exponential function

$$\phi_q(t) = f_q^c \exp[-(t/\tau_q)^{\beta_q}]. \tag{36}$$

However, both τ_q and β_q are found to be q-dependent in solutions of the MCT equations, a result also confirmed by computer simulations and neutron scattering experiments. Since the von Schweidler exponent b is independent of q, there cannot be any simple relation, in general, between b and β. An exception occurs for $q \to \infty$ where Fuchs has shown that equation (36) is exact, with $\beta(q \to \infty) = b$ [20]. Note that the α-scaling (equation (35)) is an asymptotic result for $(T - T_C)/T_C \ll 1$, and its domain of validity is not known. From reference [16], however, it is known that the range of validity of the asymptotic α-relaxation results is much larger than that of the β-relaxation results, accounting for the general validity of time–temperature superposition for α-relaxation. For temperatures far above T_C, β may either increase or decrease with increasing T without violating the asymptotic MCT predictions.

Finally, we consider the temperature dependence predicted by MCT for the α-relaxation time τ. From equations (25) and (28*a*), and the form of $g_-(t/t_\sigma) = -B(t/t_\sigma)^b$ in the von Schweidler regime, one has

$$\phi_q^{(b)}(t) - f_q^c \propto \sqrt{|\sigma|}\left(\frac{t}{t_\sigma}\right)^b. \tag{37}$$

But

$$\sqrt{|\sigma|}\left(\frac{t}{t_\sigma}\right)^b = |\sigma|^{1/2}\left(\frac{t}{t_0}|\sigma|^{1/2a}\right)^b = \left(\frac{t}{t_0}|\sigma|^{1/2a}|\sigma|^{1/2b}\right)^b \tag{38}$$

so the von Schweidler decay region must move to longer times as T decreases following

$$t'_\sigma = B^{-1/b} t_0/|\sigma|^\gamma \tag{39a}$$

with

$$\gamma = \frac{1}{2a} + \frac{1}{2b}. \tag{39b}$$

(B is a number of order unity determined by λ.) Since the α-relaxation must smoothly continue the von Schweidler decay, MCT predicts that the α-relaxation time τ has the same temperature dependence as t'_σ:

$$\tau(T) = \tau_0(T - T_C)^{-\gamma} \qquad (T > T_C). \tag{40}$$

Plots of $(1/\tau)^{1/\gamma}$ versus T exhibit linear behaviour as predicted by equation (40) over considerable temperature ranges, extrapolating to zero at a T_C that is generally compatible with the T_C deduced from the β-relaxation analysis. However, on approaching T_C, plots of experimental $(1/\tau)^{1/\gamma}$ data generally deviate from the linear extrapolation, exhibiting upward curvature. This observation indicates that, in structural glasses, the complete structural arrest at T_C predicted by the idealized MCT does not occur.

3.5. Extended MCT

The ideal glass transition predicted by the idealized MCT is not observed in real glass-forming materials (with the possible exception of colloidal glasses). Instead, $\phi_q(t)$ always relaxes from the plateau to zero after a sufficiently long time. Non-ergodicity is therefore only observed on timescales short compared to the final relaxation time. At very low temperatures, however, the final relaxation becomes glacial, unobservable on any practical experimental timescale.

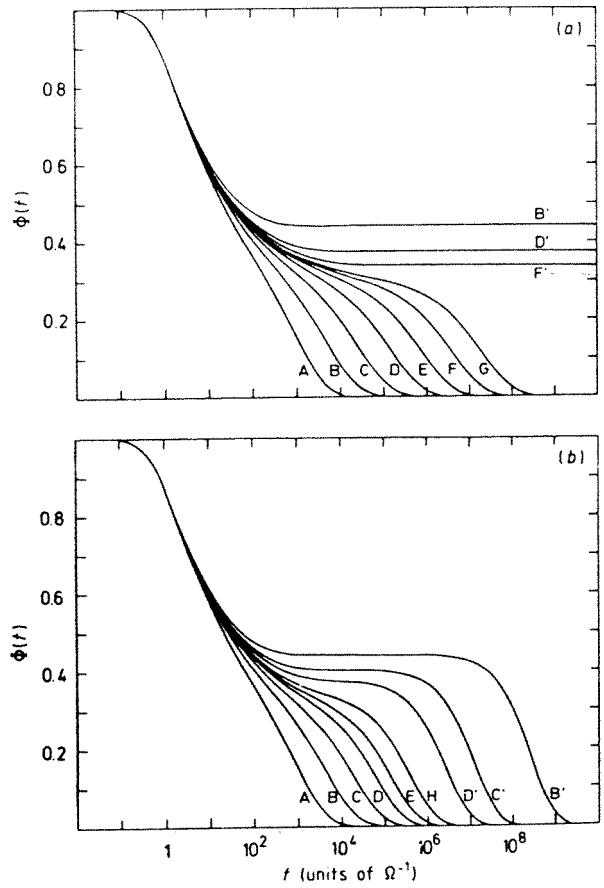

Figure 8. Correlation functions $\phi(t)$ (this page) and susceptibility spectra $\chi''(\omega)$ (facing page) for a schematic model of the idealized MCT (a) and the corresponding extended model (b). Curves A–G are for $T > T_C$ while curves F′–B′ are for $T < T_C$. (From reference [23].)

The singularity at T_C predicted by MCT results from restricting the memory kernel (equation (22)) to the dominant terms which are pairs of density-fluctuation modes. In the next-to-leading-order terms in $m_q(t)$, current modes occur, as first shown by Das and Mazenko [21] and by Götze and Sjögren [22, 23]. When these terms are included, equation (26) for $G(t)$ is replaced by

$$\lambda G^2 + \sigma - \delta t = \frac{\mathrm{d}}{\mathrm{d}t}\int_0^t G(t-t')G(t')\,\mathrm{d}t' \tag{41}$$

which differs from equation (26) only by the term $-\delta t$. This term is an approximation for the complete effect of the current terms which resembles phonon-assisted activated hopping processes in crystals. Even if the hopping parameter δ is small, the term $-\delta t$ will always dominate at sufficiently long times, causing $G(t)$ to eventually fall below zero, initiating the α-decay.

Figure 8 shows the correlation functions $\phi_q(t)$ (left) and the corresponding susceptibility spectra $\chi''(\omega)$ (right) computed for a schematic MCT model for the idealized ($\delta = 0$, top) and extended (bottom) versions. In this model, only one correlator ϕ is considered, and the right-hand side of equation (22) is replaced by a polynomial $v_1\phi(t) + v_2\phi^2(t)$. Note that the

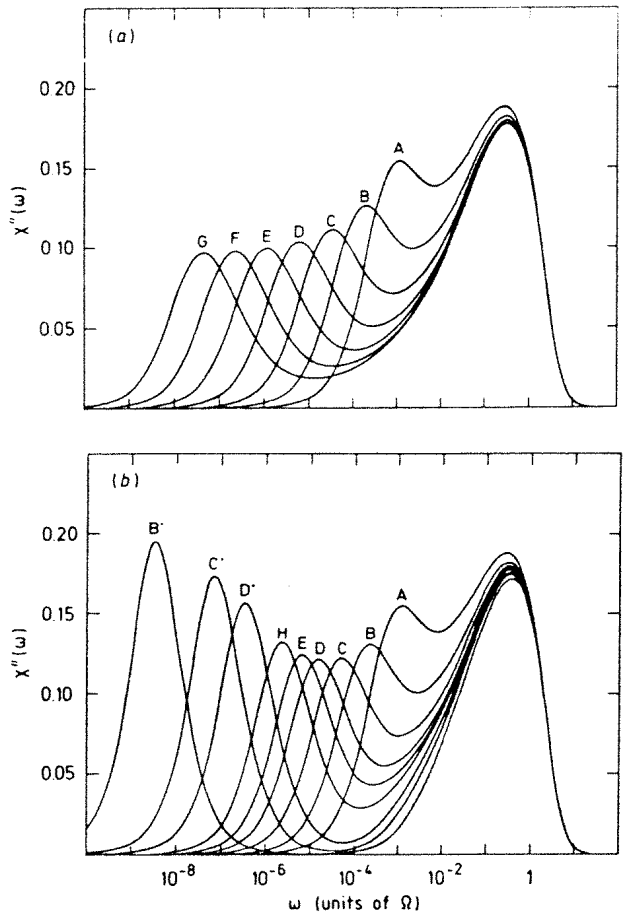

Figure 8. (Continued)

α-peak in $\chi''(\omega)$ disappears at T_C for the idealized MCT but is present at all temperatures for the extended MCT.

The $\chi''(\omega)$ spectra for $T > T_C$ are changed somewhat by hopping effects, especially at low frequencies where the long-time properties of $\phi_q(t)$ are most important. Below T_C however, as the dominant dynamics crosses over from cage-effect hydrodynamics to activated transport, the spectra are strongly modified. The 'knee' in figure 6(b) can be modified or eliminated [24], and the cusp in $f_q(T)$ (equation (24)) can be broadened. We recall that the knee is a consequence of the crossover from the critical decay to the horizontal plateau in $\phi(t)$ versus t. If another decay process (such as activated hopping) causes $\phi(t)$ to decay before the plateau is fully developed, the knee will be absent. This appears to be the case for most glass-forming materials, although not for colloidal glasses. Figure 9 illustrates the evolution of the susceptibility spectrum with decreasing T when hopping is included. Note that the minimum persists, even at the lowest temperatures.

In the original (idealized) version of MCT, T_C is a critical temperature at which complete structural arrest occurs. In the extended version, the singularity is avoided, and T_C represents a crossover temperature between the high-temperature regime dominated by liquid-like cage effects, and the low-temperature regime dominated by solid-like activated hopping processes.

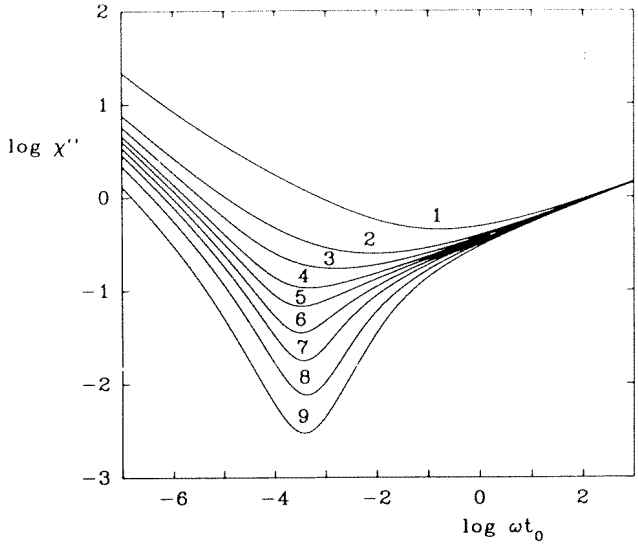

Figure 9. Susceptibility spectra $\chi''(\omega)$ for temperatures decreasing from curve 1 to curve 9 with hopping included, illustrating the persistence of the minimum at $T < T_C$. Curves 1–3 correspond to $T > T_C$, curve 4 to $T = T_C$, and curves 5–9 to $T < T_C$. (From reference [24].)

The extended version of MCT represented by equation (41) is a first approximation. A complete MCT description of the dynamics for $T < T_C$ has not yet been formulated.

4. Summary and conclusions

The idealized MCT equations are currently being extended by several groups to include more realistic intermolecular potentials as well as orientational effects. These extensions should eventually permit more complete comparison of experimental data with full MCT predictions rather than with just the results of asymptotic expansions. So far, however, almost all tests of MCT have been carried out using the MCT asymptotic predictions discussed in the preceding sections. These tests, discussed in detail by W Götze, include:

(1) The cusp in $f_q(T)$ at T_C (equation (24)).

(2) The power-law critical decay of $\phi_q(t)$ towards the plateau.

(3) The von Schweidler power-law decay of $\phi_q(t)$ away from the plateau.

(4) Scaling of correlation functions and susceptibility spectra in the β-relaxation region and the temperature dependence of the scaling time t_σ (equations (28) and (29)).

(5) The factorization property (q-independent time dependence) in the β-relaxation regime (equation (25)).

(6) Scaling of the α-relaxation and temperature dependence of the second scaling time τ (equations (35) and (39)).

(7) The evolution with temperature of $\phi_q(t)$ and $\chi_q''(\omega)$.

Comparison of experimental data with these predictions is a subtle procedure and the results are not always clear cut. Nevertheless, a growing body of experimental data and computer simulation results indicate that the essential features of the dynamics of liquids approaching the liquid–glass transition is correctly contained in the MCT description, at least for temperatures above T_C. Elaboration of the theory for $T < T_C$ remains to be pursued in the

future.

Acknowledgments

I thank W Götze for suggestions concerning this article, and M Fuchs, M Mayr, T Franosch, A Singh, and T Voigtmann for many helpful discussions and for assistance in preparing the figures. I also thank the Technical University of Munich and the Alexander von Humboldt Foundation for hospitality and support for an extended visit to the TUM during the preparation of this article. This research was supported by NSF Grant No DMR-9616577.

Appendix. Elements of the MCT asymptotic β-relaxation analysis

This appendix is based on references [25] and [1].

For the following discussion, we consider a schematic MCT model with a single correlator $\phi(t)$. The equation of motion and the memory function are given by

$$\ddot{\phi}(t) + \Omega^2\phi(t) + \int_0^t M(t-t')\dot{\phi}(t')\,\mathrm{d}t' = 0 \tag{A.1}$$

$$M(t) = \gamma\delta(t) + \Omega^2 m(t) \tag{A.2}$$

$$m(t) = F[\phi(t)] = v_1\phi(t) + v_2\phi^2(t) + \cdots \tag{A.3}$$

where v_1 and v_2 are smoothly decreasing functions of temperature or increasing functions of density.

Laplace transformation of equation (A.1) with the Laplace transform convention

$$L[\phi(t)] = \mathrm{i}\int_0^\infty \mathrm{e}^{\mathrm{i}zt}\phi(t)\,\mathrm{d}t = \phi(z)$$

yields

$$\phi(z) = \frac{-1}{z - \dfrac{\Omega^2}{z + \gamma + \Omega^2 m(z)}}. \tag{A.4}$$

As $T \to T_C$ from above (or $\rho \to \rho_C$ from below), solutions to the MCT equations extend to longer and longer times (see figure 3), exhibiting a plateau at a level $0 < f^c < 1$, with the result that $\phi(z=0)$, which is the integral of $\phi(t)$, diverges. Therefore, for small z, $\phi(z)$ and, via equation (A.3), $m(z)$ as well become very large. In the second term in the denominator of equation (A.4), z and γ can then be ignored in comparison to $\Omega^2 m(z)$. In this limit, equation (A.4) becomes

$$\phi(z) = \frac{-1}{z - \dfrac{1}{m(z)}}. \tag{A.5}$$

Inverse Laplace transformation of equation (A.5) gives

$$\int_0^t m(t-t')\phi(t')\,\mathrm{d}t' = \int_0^t [m(t') - \phi(t')]\,\mathrm{d}t'. \tag{A.6}$$

Equation (A.6) applies for the liquid close to T_C and also for the glass, and is the starting point for the asymptotic analysis. The $t \to \infty$ limit of $\phi(t)$ is the non-ergodicity parameter f. For $\rho < \rho_C$, $f = 0$; for $\rho = \rho_C$, $f = f^c$; for $\rho > \rho_C$, $f > f^c$.

We next let $\phi(t) = f + (1 - f)G(t)$ and $\rho = \rho_C(1 + \epsilon)$ and carry out a power series expansion of equation (A.6) using both ϵ and $G(t)$ as small parameters. Since this analysis is for $\phi(t)$ close to the plateau, it applies—by definition—only to the β-relaxation region.

For the zeroth-order approximation, let $\phi(t) = f$ and $F[\phi] = F(f)$. Then equation (A.6) becomes

$$F(f)ft = [F(f) - f]t \to F(f)(1 - f) = f \tag{A.7}$$

so

$$F(f) = \frac{f}{1 - f}. \tag{A.8}$$

Equation (A.8) determines the non-ergodicity parameter f.

Consider, for example, the simplest schematic model, the F_2- (Leutheusser) model:

$$m(t) = F[\phi(t)] = V\phi^2(t) \tag{A.9}$$

$$\frac{f}{1 - f} = Vf^2 \to f = \frac{V \pm \sqrt{V^2 - 4V}}{2V} \qquad \text{or} \qquad f = 0. \tag{A.10}$$

For $V < 4$, the only real solution to equation (A.10) is $f = 0$. For $V = 4$, a second real solution appears:

$$f(V = 4) = f^c = \frac{1}{2} \tag{A.11}$$

which locates the bifurcation at $V_C = 4$. For $V > 4$,

$$f = \frac{1}{2} \pm \frac{1}{4}\sqrt{V - V_C} \tag{A.12}$$

for which only the upper (+) solution is physical. Assuming that V increases linearly with ρ (or decreases linearly with T) then gives the square-root cusp result of equation (24) in the main text.

Next, $F[\phi(t)]$ is expanded in both G and ϵ for $f = f^c$:

$$F[\phi(t)] = F^c[f^c] + \left[\frac{\partial F^c}{\partial \rho}\right]\rho_C\epsilon + \left[\frac{\partial F^c}{\partial f}\right](1 - f^c)G + \frac{1}{2}\left[\frac{\partial^2 F^c}{\partial f^2}\right](1 - f^c)G^2 + \cdots \tag{A.13}$$

where the derivatives are evaluated at $\epsilon = 0$ and $\phi(t) = f^c$. The zeroth-order term in the resulting expansion of equation (A.6) is equation (A.8) for the critical point. The first-order term vanishes, and this is the condition for the critical point. The second-order term gives

$$\int_0^t [\lambda G^2(t') + \sigma]\, \mathrm{d}t' = \int_0^t G(t - t')G(t')\, \mathrm{d}t' \tag{A.14}$$

with $\sigma \propto \epsilon$ and $\lambda = \frac{1}{2}(\partial^2 F/\partial f^2)(1 - f^c)^3$. Equation (A.14) gives equation (26) in the main text which defines the beta-correlator $G(t)$. At $\rho = \rho_C$ (or $T = T_C$), $\sigma = 0$, and equation (A.14) becomes

$$\lambda \int_0^t G^2(t')\, \mathrm{d}t' = \int_0^t G(t - t')G(t')\, \mathrm{d}t'. \tag{A.15}$$

Consider a power-law trial solution for equation (A.15):

$$G(t) = \gamma t^x \tag{A.16}$$

with which equation (A.15) is

$$\gamma^2\lambda \int_0^t (t')^{2x}\, \mathrm{d}t' = \gamma^2 \int_0^t (t - t')^x (t')^x\, \mathrm{d}t'. \tag{A.17}$$

For equation (A.17) to be satisfied, λ and x must be related by

$$\lambda = \frac{\Gamma^2(1+x)}{\Gamma(1+2x)} \tag{A.18}$$

where $\Gamma(x)$ is the gamma function.

There are two solutions to equation (A.18) for $1/2 \leqslant \lambda \leqslant 1$: $x = b$ with $0 < b < 1$, and $x = -a$ with $0 < a \leqslant 0.395$. This is the origin of the critical decay law (equation (27) in the main text) and of the gamma-function relation between the critical exponents a and b of MCT. The derivation of equation (A.14) can be generalized to the full MCT equations, but the proof and resulting formulae for σ and λ are somewhat more complicated [3].

References

[1] Bengtzelius U, Götze W and Sjölander A 1984 *J. Phys. C: Solid State Phys.* **17** 5915
[2] Leutheusser E 1984 *Phys. Rev.* A **29** 2765
[3] Götze W 1991 *Liquids, Freezing and Glass Transition* ed J-P Hansen, D Levesque and J Zinn-Justin (Amsterdam: North-Holland) p 289
[4] Götze W and Sjögren L 1992 *Rep. Prog. Phys.* **55** 241
[5] Cummins H Z, Li Gen, Hwang Y H, Shen G Q, Du W M, Hernandez J and Tao N J 1997 *Z. Phys.* B **103** 501
[6] Mountain R D 1966 *Rev. Mod. Phys.* **38** 205
Mountain R D 1966 *J. Res. NBS* A **70** 207
Mountain R D 1968 *J. Res. NBS* **72** 95
[7] Axe J D, Shapiro S M and Shirane G 1974 *Anharmonic Lattices, Structural Transitions and Melting* ed T Riste (Amsterdam: Noordhof-Leiden) p 23
[8] Winterling G 1975 *Phys. Rev.* B **12** 2432
[9] Sokolov A P, Novikov V N and Strube B 1997 *Phys. Rev.* B **56** 5042
Novikov V N, Sokolov A P, Strube B Surotsev N V, Duval E and Mermet A 1997 *J. Chem. Phys.* **107** 1057
[10] Cowley R A 1963 *Adv. Phys.* **12** 421
Cowley R A 1965 *Phil. Mag.* **11** 673
Cowley R A 1980 *Adv. Phys.* **29** 1
[11] Silberglitt R 1972 *Solid State Commun.* **11** 247
[12] Berne B J and Pecora R 1976 *Dynamic Light Scattering* (New York: Wiley–Interscience) ch 11
[13] Kawasaki K 1970 *Ann. Phys., NY* **61** 1 and references cited therein
[14] Fixman M 1960 *J. Chem. Phys.* **33** 1357
Fixman M 1960 *J. Chem. Phys.* **33** 1363
Fixman M 1962 *J. Chem. Phys.* **36** 310
Fixman M 1964 *Adv. Chem. Phys.* **6** 175
Botch W D and Fixman M 1965 *J. Chem. Phys.* **42** 199
[15] Bengtzelius U 1986 *Phys. Rev.* A **34** 5059
[16] Franosch T, Fuchs M, Götze W, Mayr M R and Singh A P 1997 *Phys. Rev.* E **55** 7153
[17] Fuchs M 1995 *Transport Theory Stat. Phys.* **24** 855
[18] Fabbian L, Götze W, Sciortino F, Tartaglia P and Thiery F 1999 *Phys. Rev.* E **59** R1347
[19] Fuchs M, Götze W and Mayr M R 1999 *Phys. Rev.* E at press
[20] Fuchs M 1994 *J. Non-Cryst. Solids* **172–174** 241
[21] Das S P and Mazenko G M 1986 *Phys. Rev.* A **34** 2265
[22] Götze W and Sjögren L 1987 *Z. Phys.* B **65** 415
[23] Götze W and Sjögren L 1988 *J. Phys. C: Solid State Phys.* **21** 3407
[24] Fuchs M, Götze W, Hildebrand S and Latz A 1992 *J. Phys.: Condens. Matter* **4** 7709
[25] Götze W 1998 *Rome Lectures* unpublished